Hindered Rotation around a C−•PH Bond: A Single-Crystal EPR Study of the Diphenyldibenzobarrelenephosphinyl Radical

Marcin Brynda, Théo Berclaz, Michel Geoffroy,* and Geetha Ramakrishnan

Department of Physical Chemistry, 30 Quai Ernest Ansermet, University of Geneva, 1211, Geneva, Switzerland

Gérald Bernardinelli

Laboratory of X-ray Crystallography, 24 Quai Ernest Ansermet, University of Geneva, 1211 Geneva, Switzerland

Received: March 26, 1998; In Final Form: June 16, 1998

A new phosphine, the diphenyldibenzobarrelenephosphine **2**, was designed to study the barrier to rotation of the P−H group around the C−•P bond. After homolytic scission of a P−H bond by radiolysis, the EPR spectrum of the resulting phosphinyl radical, trapped in a single crystal of **2**, was studied at 77 K and at room temperature. The directions of the ^{31}P hyperfine eigenvectors were compared with the bond orientations of the undamaged compound as determined from its crystal structure. The temperature dependence of the EPR spectrum was analyzed by using the density matrix formalism; this showed that interaction between the phosphinyl hydrogen and the phenyl ring bound to the ethylenic bond is determinant for explaining the potential energy profile. DFT investigations are consistent with these experimental results.

Introduction

Whereas a large variety of spectroscopic techniques are well-suited to the study of hindered rotation in diamagnetic molecules,[1] investigation of the motion around a RA•−BR′ bond, where the atom A bears an unpaired electron, is considerably more problematic. We have recently reported[2] that radical derivatives of 9-substituted triptycenes potentially offer a good opportunity for such measurements: after radiolytic scission of a P−H bond in **1** (Scheme 1) the temperature dependence of the single-crystal EPR spectrum of **R1** is directly dependent upon the rotation barrier around the C−•PH bond.

SCHEME 1

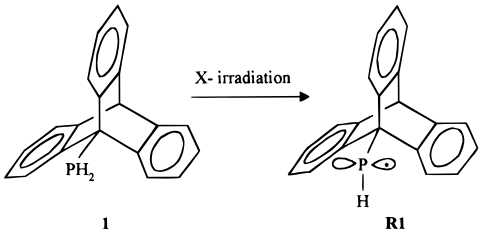

1 **R1**

The question is to know to what extent this motion, and therefore the EPR spectrum, is sensitive to structural modifications of the triptycyl moiety. We have therefore synthesized the novel compound **2**, which, in contrast with **1**, has no C_3 axis. We show that the corresponding radiogenic phosphinyl radical **R2** gives rise to an EPR spectrum whose temperature dependence considerably differs from that observed for **R1**.

From an analysis that combines a density matrix simulation of the spectra recorded for **R2**, the crystallographic parameters measured on **2**, and functional density calculations performed on **R2′**, we have obtained a detailed description of the rotation of the P−H group around the C−•P bond in the solid state. This method appears to be particularly informative about the steric hindrance caused by the presence of such a moderately cumbersome group as a phenyl ring.

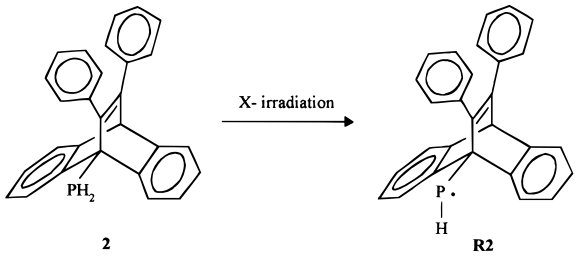

2 **R2**

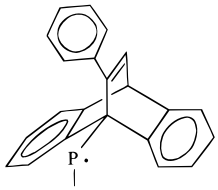

R2'

Experimental Section

To simplify the EPR analysis, spectra were obtained after deuteration of the phosphinyl group of **2** (**D-2**), and for the sake of comparison new measurements were carried out on the deuterated phosphine **1** (**D-1**).

Syntheses. As shown in Scheme 2, **2** was synthesized by a direct Diels−Alder addition[3] followed by lithiation of the adduct and the subsequent reduction of dichlorophosphine. All experiments were performed under dry N_2 atmosphere.

*9-Bromodiphenyldibenzobarrelene (**2a**).* A glass tube containing 4 g of bromoanthracene and 3.1 g of diphenylacetylene dissolved in 40 mL of triglyme was sealed and heated at 235 °C for 48 h in an autoclave. After cooling, 300 mL of diethyl ether was added to the dark brown solution. The residual

10.1021/jp9816519 CCC: $15.00
Published on Web 10/02/1998

SCHEME 2

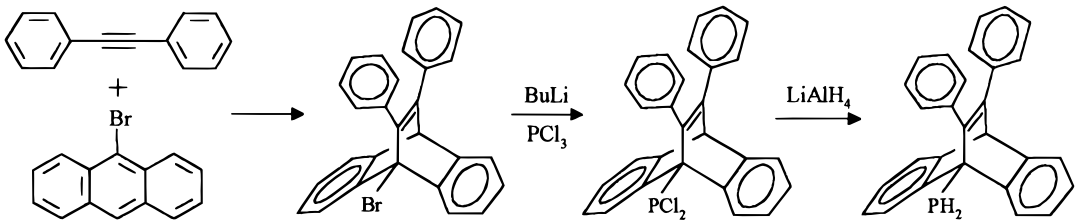

2a **2b** **2**

solvent was extracted with three times 100 mL of water, and after the usual workup the resulting brown oily solution was quickly poured into 200 mL of hexane cooled to 0 °C. The resulting yellow crystalline powder was dried under vacuum and recrystallized from an ether/hexane mixture. Yield: 1.37 g [21%]. MS-M^+: 436; 355; 256; 178; 151, Mp = 160 °C, ^{1}H-RMN 5.45 (s, 1H), 6.82 (m, 2H), 6.99 (m, 2H), 7.15 (m, 10H), 7.79 (m, 2H) ppm.

9-Diphenyldibenzobarrelenephosphine (2). *n*-BuLi (3.15 mL) (1.6 M in hexane) was slowly added, at −100 °C, to a solution containing 1.8 g of **2a** in 30 mL of dry THF. After 20 min the temperature was allowed to slowly rise and then maintained at −65 °C for 30 min. Then the mixture was cooled to −80 °C, and 0.6 mL of PCl_3 was added all at once. The solution was heated and refluxed for 1 h. After cooling, the mixture was slowly poured, at 0 °C, in a suspension of 0.3 g of $LiAlH_4$ in dry hexane. After additional reflux (2 h) a few drops of HCl/H_2O were carefully added to the solution. The solution was then extracted with 3 × 30 mL of ether, washed, dried, and evaporated. The final product was separated by silica gel chromatography using hexane/ether (9:1) as an eluant. Yield: 63% (1 g).

MS-M^+: 388, Mp = 141 °C, ^{1}H-RMN 2.75; 3.76 (d, 2H, J_{PH} = 201 Hz), 5.47 (s, 1H), 6.84 (m, 2H), 6.99−7.25 (m, 12 H), 7.43 (m, 2H), 7.56 (m, 2H) ppm. ^{31}P-RMN: −152 ppm, J_{P-H} = 201 Hz.

Deuteration of 2. The procedure was similar to that described for the undeuterated compound. However, **2b** was reacted with $LiAlD_4$, and, after refluxing, two drops of DCl/D_2O were added to the reaction mixture. After extraction and partial evaporation of the solution, yellow crystals grew on keeping the solution one night at 0 °C. These crystals were dissolved in THF, and the deuterated compound **D-2** was isolated by chromatography on deuterated alumina[4] with hexane/ether as an eluant. Yield: 39% (0.62 g).

Crystallographic Data and Structure Determination of 2. $C_{28}H_{21}P$, M_r = 388.4; μ = 1.254 mm^{-1}, $F(000)$ = 816, d_x = 1.26 g·cm^{-3}, orthorhombic, $P2_12_12_1$, Z = 4, a = 9.890(1), b = 13.654(2), c = 15.148(1) Å, V = 2045.6(4) Å^3 from 23 reflections (46° < 2θ < 53°), colorless prism 0.08 × 0.20 × 0.26 mm mounted on a quartz fiber with RS3000 oil to prevent degradation. Cell dimensions and intensities were measured at 200 K on a STOE Stadi4 diffractometer with graphite-monochromated Cu Kα radiation (λ = 1.5418 Å), ω−2θ scans, scan width 1.11° + 0.35 tg θ, and scan speed 0.06 deg/s. Two reference reflections measured every 45 min showed variation less than 2.5 σ (I). 3° < 2θ < 110°; 0 < h < 10; 0 < k < 14; 0 < l < 15 and all antireflections of these; 3638 measured reflections, 2505 unique reflections of which 2275 were observable ($|F_o| > 4\sigma(F_o)$); R_{int} for 1133 equivalent reflections 0.026. Data were corrected for Lorentz and polarization effects and for absorption [5] (A^* min, max = 1.099, 1.343). The structure was solved by direct methods using MULTAN 87;[6] all other calculations used the XTAL[7] system and ORTEP[8] programs. The chirality/polarity of the structure was refined, and the absolute structure parameter[9] converges to x = 0.02 (5). The structure was refined by full-matrix least-squares, based on $|F|$, using a weight of $1/(\sigma^2(F_o) + 0.0001(F_o^2))$ and gave final values R = 0.037, ωR = 0.035, and S = 2.21(5) for 330 variables and 2275 contributing reflections. The mean and maximum shift/error on the last cycle was 0.34 × 10^{-3} and 0.21 × 10^{-2} respectively. All coordinates of hydrogen atoms were observed and refined with a fixed value of isotropic displacement parameters (U = 0.05 Å^2). Three atomic sites have been observed, for the hydrogen atoms bonded to the phosphorus. As shown by the difference electron density map, these hydrogen atoms have been refined with population parameters of 0.8, 0.8, and 0.4 (Σ of populations = 2) for H(01), H(02), and H(03) respectively (Figure 1). The final difference electron density map showed a maximum of +0.17 and a minimum of −0.22 e Å^{-3}.

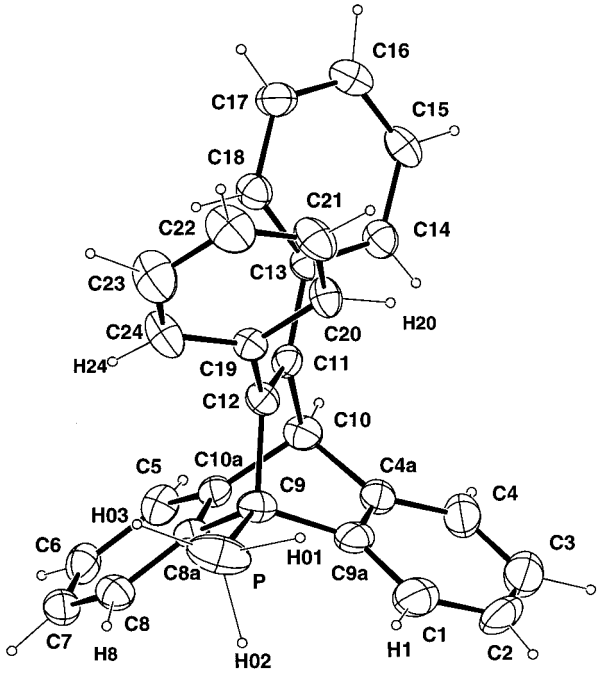

Figure 1. Perspective view of the 9-diphenyldibenzobarrelenephosphine **2** with the atom numbering. Ellipsoids are represented with 40% probability level.

EPR Measurements. In a typical experiment a large single crystal of **2** (or **D-2** or **D-1**), obtained by slow evaporation of a solution in a hexane/diethyl ether (9:1) mixture, was X irradiated at room temperature under vacuum for 2 h (tungsten anticathode, 30 mA, 30 kV). The irradiated crystal was then glued on a small brass sample holder designed to allow rotation of the crystal around the three crystallographic axes (the experimental

TABLE 1: Selected Bond Lengths (Å), Bond Angles, and Torsional Angles (deg) for the 9-Diphenyldibenzobarrelenephosphine 2

P−C(9)	1.862(5)	C(10)−C(10a)	1.533(6)
C(4a)−C(9a)	1.401(8)	C(10)−C(11)	1.537(6)
C(4a)−C(10)	1.515(8)	C(11)−C(12)	1.338(6)
C(8a)−C(9)	1.519(6)	P−H(01)	1.37(5)
C(8a)−C(10a)	1.397(7)	P−H(02)	1.37(5)
C(9)−C(9a)	1.554(7)	P−H(03)	1.37(4)
C(9)−C(12)	1.554(6)		
H(01)···H(1)	2.31(7)	H(01)···H(20)	3.74(6)
H(02)···H(1)	2.26(6)	H(02)···H(8)	2.46(6)
H(03)···H(8)	2.8(1)	H(03)···H(24)	2.5(1)
P−C(9)−C(8a)	112.6(3)	C(9)−P−H(01)	95(2)
P−C(9)−C(9a)	115.4(3)	C(9)−P−H(02)	93(2)
P−C(9)−C(12)	112.2(3)	C(9)−P−H(03)	114(2)
C(8a)−C(9)−C(9a)	104.0(4)	H(01)−P−H(02)	86(3)
C(8a)−C(9)−C(12)	107.3(4)	H(01)−P−H(03)	127(3)
C(9a)−C(9)−C(12)	104.4(4)	H(02)−P−H(03)	132(3)
H(01)−P−C(9)−C(8a)	160(2)	H(02)−P−C(9)−C(12)	−165(2)
H(01)−P−C(9)−C(9a)	40(2)	H(03)−P−C(9)−C(8a)	−65(3)
H(01)−P−C(9)−C(12)	−79(2)	H(03)−P−C(9)−C(9a)	175(3)
H(02)−P−C(9)−C(8a)	73(2)	H(03)−P−C(9)−C(12)	56(3)
H(02)−P−C(9)−C(9a)	−46(2)		

EPR reference axes *X*, *Y*, *Z*, for **2** and **D-2** are respectively aligned along the *a*, *b*, *c* directions). To prevent any chemical alteration in the irradiated compound, the crystal was then coated with an inert adhesive polymer.

The EPR spectra were recorded on a Bruker 200D spectrometer (X-band) equipped with an AST computer recording unit and a VT1100 temperature controller. The angular variations of the spectra, in three perpendicular planes, were obtained at 300 K and at 77 K. The EPR tensors were determined by using an optimization program that calculates the position of the signals with second-order perturbation theory.

As described in more detail in ref 2, the EPR spectra were simulated by using the density matrix formalism.[10] The intensity of the EPR signal was calculated as $I(\omega) = \mathrm{Re}(S^{+}(\omega)) = \mathrm{Tr}(\rho S^{+}) = \mathrm{Tr}(\rho^{-+})$. All the calculations were performed in Liouville space by summing the elements of the vector $\rho^{-+} = iI_o\,(U^{-1}\Lambda U - i\omega 1)^{-1}P$ where Λ is a diagonal matrix and P is a vector containing the populations of the various configurations. In addition to the transition values and the $-1/T_2$ terms, the elements of the matrix $L = (U^{-1}\Lambda U - i\omega 1)$ contain the rate constants k_{ij}. For **R2**, three configurational sites (*J*, *K*, *L*) are present; at a given temperature each site is characterized by its population $P_i (i = j, k, l)$ and by its exchange parameters with the two other sites: $k_{ih} = P_h \cdot k_{hi}/P_i$ (with $h \neq i$, $h = j, k, l$). The correlation time τ is related to k as $\tau = (2\pi \times 2.8 \times 10^6 k)^{-1}$. The temperature dependence of the spectra was analyzed by determining, for each temperature, the set of k_{ij} values that leads to a good simulation of the experimental spectrum.

Quantum Mechanical Calculations. DFT calculations were carried out on a Silicon Graphics computer (IRIS 4D) using the GAUSSIAN94 package.[11] All the results were obtained with a 3-21G* basis set.

Results

Crystal Structure of 2. Selected geometrical parameters are reported in Table 1. No significant difference in the geometrical parameters are observed with the analogous 9-phosphinyltriptycene compound.[2] Nevertheless, it should be noted that in **2** the bond length of the C(11)−C(12) bridge is significantly shorter than in the C(4a)−C(9a) and C(8a)−C(10a) phenyl bridges. The dihedral angles between the mean planes of the central barrelene skeleton are 118.8, 119.1, and 122.2°. The two phenyl rings at C(11) and C(12) are conrotatory oriented (C(9)−C(12)-C(19)−C(20) = 113.1(5)° and C(10)−C(11)-C(13)−C(18) = 145.1(5)°) and show a slide deviation of C(13) (0.126(8) Å) and C(19) (0.109(8) Å) out of the mean plane of the C(9)−C(10)-C(11)−C(12) bridge toward the C(1)−C(9a) phenyl ring.

TABLE 2: g, ^{1}H, and ^{31}P Coupling Tensors Measured at 300 K for Radical R2

		principal axes[a]		
tensor	principal values	λ	μ	ν
g	2.0050	0.1846	−0.7389	−0.6480
	2.0072	0.9748	0.2219	0.0248
	2.0109	0.1255	−0.6362	0.7612
^{31}**P**	527	−0.4189	0.5842	0.6951
	293	−0.9039	−0.1959	−0.3801
	39	0.0859	0.7876	−0.6102
^{1}**H**	61	−0.0899	−0.8113	0.5776
	37	−0.1259	−0.5660	−0.8147
	33	0.9879	−0.1460	−0.0513

[a] Principal axes for the other sites are obtained from the symmetry operations: $\bar{\lambda}, \mu, \nu$; $\lambda, \bar{\mu}, \nu$; $\lambda, \mu, \bar{\nu}$.

As mentioned in the crystallographic experimental section, three atomic sites have been observed for the hydrogen atoms bonded to the phosphorus showing staggered conformations relative to the barrelene moiety. The coordinates of these hydrogen atoms have been refined with weak restraints on the P−H bond lengths. The population parameters observed for these atomic sites show one major rotamer (60%) and two equally populated (20%) minor rotamers. For the major conformation, C−P−H and H−P−H bond angles are in good agreement with analogous phosphine compounds[12] despite short interatomic interactions with H(1) (Table 1). In the crystal structure and for the temperature of measurement (200 K), we can assume that no free rotation occurs about the C−P bond. This assumption seems to be confirmed by the anisotropy of the displacement parameters observed on the phosphorus atom where the main displacement is oriented parallel to the P−H(03) direction (see Figure 1). Both minor rotamers involving H(03) show a significant opening of the C−P−H and H−P−H bond angles.

EPR Results. *Spectra Obtained with a Single Crystal of **2**.* When the magnetic field lies in an EPR reference plane (*X*, *Y*, *Z*), the EPR spectrum obtained at room temperature with an X irradiated single crystal of **2** is composed of four lines marked A and of four lines marked B (see Supporting Information); each of these subspectra exhibits hyperfine coupling with a ^{31}P nucleus and a proton. The angular variations of these signals lead to the **g**, ^{1}**H** and ^{31}**P** hyperfine tensors given in Table 2. In accord with the crystal structure that indicates the presence of four molecules per cell, the radicals are trapped along four orientations; each signal results from the overlap of two lines since the EPR reference planes are perpendicular to the C_2 axes present in the structure. On all spectra, a line, marked T, is observed around $g = 2.002$ and is probably due to the trapping of a radical resulting from the homolytic scission of the C(10)−H bond.

The spectrum is highly temperature sensitive between 100 and 240 K. At 77 K, multiple and partial overlaps of lines occur and make the resulting pattern so complex that, for some orientations, the transitions cannot be identified. This was not unexpected since, in addition to the four orientations of the phosphinyl radical present in the unit cell, freezing the motion of the PH group around the C−P bond gives rise, a priori, to

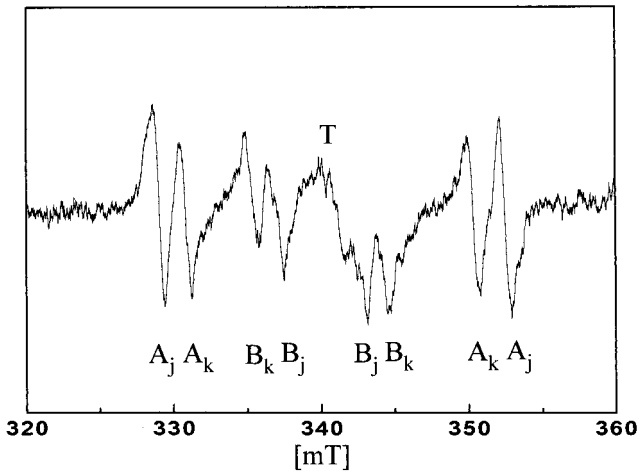

Figure 2. EPR spectrum obtained at 77 K with an X irradiated single crystal of **D-2** (H_o lies in the *ab* plane, 10° from the *a* axis).

three new sets of **g** and ^{31}**P** and ^{1}**H** hyperfine tensors. This difficulty was overcome by studying the deuterated compound.

*EPR Spectra of Deuterated **2**.* An EPR spectrum obtained at room temperature with an X irradiated single crystal of **D-2** exhibits hyperfine coupling with a ^{31}P nucleus only. The angular dependence of this spectrum leads to **g** and ^{31}**P** hyperfine tensors that are identical with those reported in Table 2 for the undeuterated radical studied at 300 K. At 77 K, when the magnetic field is oriented in the EPR reference planes, the spectrum (Figure 2) exhibits a maximum of eight lines due to additional nonequivalent orientations of the trapped radical. The subspectrum A gives rise to "configuration sites" A_j and A_k, and the subspectrum B generates B_j and B_k. The angular dependence of these signals lead to the tensors given in Table 3. It is worthwhile mentioning some geometric properties measured at low temperature: (1) the $^{31}P-T_{||}$ principal axes of the two molecular sites make an angle of 110.3°, (2) all the $^{31}P-T_{||}$ principal axes are oriented perpendicular to the crystallographic C−P direction, and (3) the $T_{||a}$ and $T_{||b}$ directions make angles of 6.4° and of 3.1° with the normals to the C(8a)C(9)P and C(12)C(9)P planes, respectively.

The number of observed transitions, their intensity, as well as their position reversibly vary with temperature between 100 and 240 K. This dependence is illustrated in Figure 3 where the spectra have been recorded when the magnetic field is aligned along the crystallographic *a* direction. For this orientation the pattern is particularly clear since the two "crystallographic sites" (A and B) are magnetically equivalent and no overlap occurs between the signals owing to the "configuration sites"(A_j and A_k, B_j and B_k).

Simulation. Simulation of the temperature dependence of the EPR spectrum by using the model of a proton exchanging between two sites that differ only by their orientation is not totally satisfactory, whereas the fitting is almost acceptable

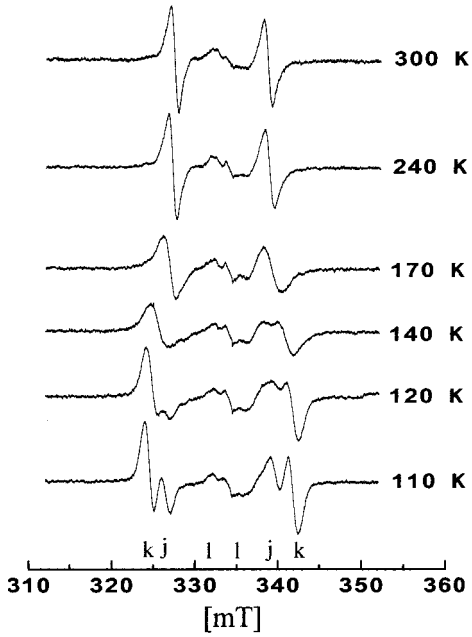

Figure 3. Temperature dependence of the experimental EPR spectrum obtained with an X irradiated single crystal of **D-2**. (H_o is aligned along the *a* axis). The lines marked k are due to an overlap of the A_k and B_k lines, j signals correspond to the overlap of the A_j and B_j lines. The calculated positions of the A_l /B_l sites are marked l.

above 180 K, it is impossible to reproduce the change in the relative intensity of the two exchanging lines (for example, A_k/A_j, in Figure 3), which is observed between 110 and 170 K. Careful examination of the spectra recorded in this temperature range shows that the change in the intensity ratio is accompanied by a change in the shape of the signal: between 110 and 130 K the broadening of the signal marked *j* is more pronounced than that of the signal marked *k*. This behavior can be simulated by assuming that a third "site", marked *l* (say A_l and B_l), with a population of 0.04 at 100 K exchanges with the configurational site *j* with a rate constant k_{jl} equal to 0.11 and with the site *k* with a constant $k_{kl} = 0.30$. The resonance positions of the A_l and B_l lines were assumed to occur at the field values calculated for a phosphinyl radical whose C(9a)C(9)PD dihedral angle is equal to 180° ($H_{\text{low field}} = 332$ mT, $H_{\text{high field}} = 334$ mT). The populations of the J and K structures were assumed to be both equal 0.48 at 100 K. At higher temperature the population numbers of J, K, L were calculated accordingly to the Boltzmann distribution and the k_{uv} ($u, v = j, k, l$) values were adjusted by simulation. In these conditions the lines *l* are never directly observed, but they are revealed by the shape modification of signals A_j, A_k (and B_j, B_k). The resulting simulations are shown in Figure 4, and the related parameters are given in Table 4.

*EPR Spectra of Deuterated **1***. The deuteration of **1** causes a drastic simplification of the low-temperature spectra and

TABLE 3: g and ^{31}P Coupling Tensors for the Radical D-2 at 77 K

		principal axes[a]		
tensor	principal values	λ	μ	ν
site j/k **g**	2.0014/2.0014	−0.5378/0.5961	−0.5403/−0.4998	−0.6472/−0.6283
	2.0047/2.0059	0.6348/0.4991	−0.7647/0.8437	0.1109/−0.1976
	2.0137/2.0147	−0.5548/0.6289	−0.3512/−0.1958	0.7542/0.7524
site j/k ^{31}**P**	865/833	−0.5095/0.6186	−0.5758/−0.4504	−0.6394/−0.6438
	34/74	0.6206/0.7800	0.2689/0.2529	−0.7366/0.5725
	25/28	0.5961/−0.0950	−0.7721/−0.8563	0.2203/0.5077

[a] Principal axes for the other sites are obtained from the symmetry operations: $\bar{\lambda}, \mu, \nu$; $\lambda, \bar{\mu}, \nu$; $\lambda, \mu, \bar{\nu}$.

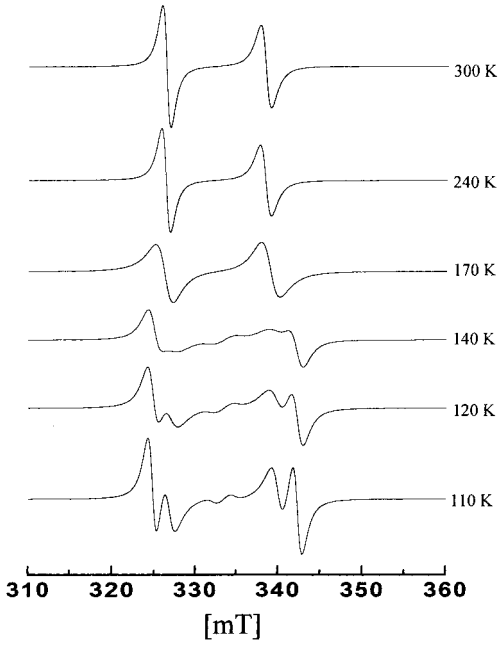

Figure 4. Simulation of the temperature dependence of the EPR spectra obtained with an X irradiated single crystal of **D-2**.

TABLE 4: Exchange Parameters and Populations Used for the Simulation of the EPR Spectra at Various Temperatures[a]

temp	k_{jl}	k_{jk}	k_{kl}	P_j	P_k	P_l
100	0.05	0.11	0.3	0.48	0.48	0.04
120	2.5	0.4	1.3	0.47	0.47	0.06
170	16.0	4.0	14.0	0.448	0.448	0.104
220	80.0	50.0	250.0	0.43	0.43	0.14
300	400.0	180.0	1800.0	0.41	0.41	0.18

[a] Additional sets of values are given as Supporting Information.

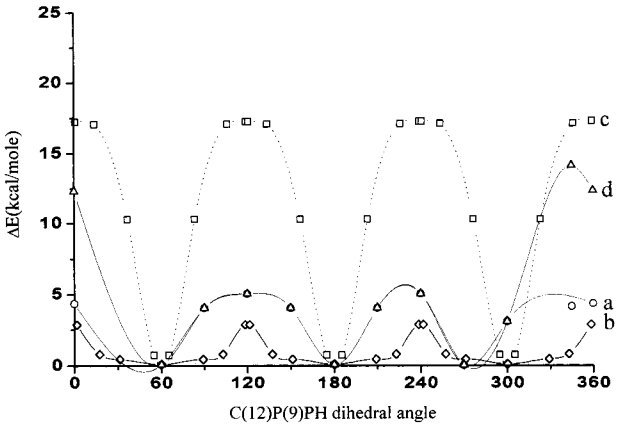

Figure 5. DFT calculated variation of the potential energy of some phosphinyl radicals as a function of the C(12)C(9)PH torsion angle: (a) **R2**; whose atomic coordinates are obtained from the crystal structure; (b) phosphinylbarrelene; (c) phosphinyltriptycene **R1**; (d) **R2′** after 15° rotation of the C(19)−C(24) ring around the C(12)−C(19) bond.

therefore a considerable improvement of the precision in the line position measurement.[13]

Quantum Mechanical Calculations. Radical **R2** is too large to be studied in depth by quantum mechanical calculations. Since the motion of the P−H bond is probably not affected by the presence of the C(13)−C(18) ring, we have used the smaller radical **R2′** as a model. To estimate the dependence of the potential energy on the orientation of the P−H bond we have therefore carried out DFT calculations on **R2′** by using the crystallographic coordinates of the carbon framework and by using for the CPH fragment the geometrical properties previously obtained by ab initio calculations on the barrelenophosphinyl radical. The resulting curve is shown in Figure 5 (curve a) together with that obtained, by the DFT method, for the barrelenephosphinyl radical (curve b); we have also performed similar calculations for the triptycylphosphinyl radical **R1** (curve c). To detect the influence of the orientation of the C(19)−C(24) phenyl ring we have performed another set of calculations by rotating the plane of this phenyl ring of 15° around the C(12)−C(19) bond. For this arbitrary structure, the potential energy as a function of the P−H orientation is also shown in Figure 5 (curve d).

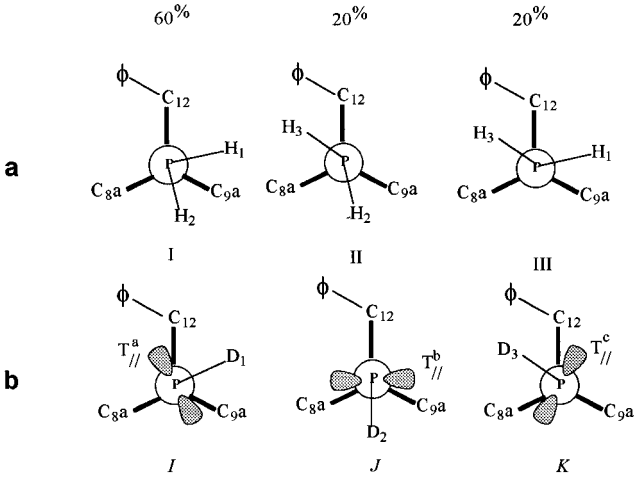

Figure 6. (a) Configurations due to the orientation of the phosphinyl group in **2** as obtained from the crystal structure. (b) Configurations due to the orientation of the •P−H bond in **R2** as obtained from the EPR analysis (ϕ represents the position of the C(19)−C(24) phenyl ring).

Discussion

The **g** and ^{31}**P** hyperfine tensors measured at 77 K for the radical trapped in a crystal of **2** (see Table 3) are totally consistent with those expected for the immobile phosphinyl radical **R2**: axial symmetry, $g_{||}$ aligned along ^{31}P−$T_{||}$ and close to 2.002, ^{31}P isotropic coupling constant A_{iso} = 310 MHz, anisotropic coupling constants: $\tau_{||}$ = 538 MHz, $\tau_{\perp}$ = 40 MHz. Moreover, as for **R1**, the parallel component of the ^{31}P hyperfine coupling is oriented perpendicular to the crystallographic C−P bond direction of the undamaged phosphine. All these properties, together with the fact that deuteration of **2** suppresses a ^{1}H coupling, show that the expected homolytic scission of the P−H bond occurs; moreover, the similarity of the tensors measured for **R1** and **R2** at 77 K clearly indicates that the EPR parameters of the motionless phosphinyl radical do not depend on the nature of the triptycene matrix.

We have already shown,[2,14] that the most stable geometry of a HP−CR_3 phosphinyl radical corresponds to the staggered configuration (HPCR dihedral angle = 180°). The salient feature of the spectra obtained with the phosphinyl radical **R2** trapped in the crystal of **2** is that each "site" detected at room temperature seems to generate only two "configurational sites" at 77 K. This is in contrast with the situation observed with a crystal of **D-1** where the P−D bond of the phosphinyl radical is blocked, at 77 K, with the same probability along the three orientations staggering the barrelene C_9−C bonds. Information about the stereochemistry of **R2** at low temperature can be obtained by examining the orientations of the magnetic phos-

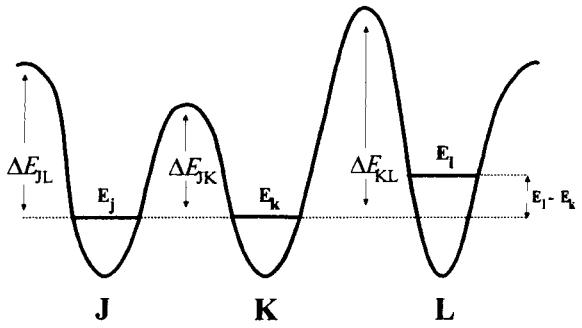

Figure 7. Schematic representation of the potential energy variation of **R2** as a function of the C(12)C(9)PH torsion angle. $\Delta E_{JL} = 2.46$ kcal·mol^{-1}, $\Delta E_{JK} = 2.37$ kcal·mol^{-1}, $\Delta E_{KL} = 2.74$ kcal·mol^{-1}, $E_K - E_J \cong 0$ kcal·mol^{-1}, $E_L - E_K = 0.5$ kcal·mol^{-1}.

phorus 3p orbital as given by the two $^{31}P-T_{||}$ principal axes: $^{31}P-T_{||}^{a}$ and $^{31}P-T_{||}^{b}$ are almost perpendicular to the planes C(8a)C(9)P and C(12)C(9)P, respectively, and imply that **R2** adopts the two configurations marked J and K in Figure 6b. In the radical, therefore, at 77 K the phosphinyl hydrogen atom never occupies the position associated with that of the atom H_3 (Figure 6a), which is the very hydrogen characterized by a small occupation parameter in the undamaged phosphine at 200 K (see crystal structure).

The fact that the position corresponding to staggered P−D and C(9)−C(9a) bonds (configuration L) is practically unoccupied at 77 K is obviously due to the presence of the phenyl ring bound to the C(12) carbon. The orientation of this ring increases the repulsion between the phosphinyl hydrogen H(3) and the hydrogen bound to C(24), and this interaction certainly destabilizes the configuration L (Figure 6b).

As shown in Table 4, the configuration L begins to be populated above 100 K, but it immediately exchanges with configuration J, whereas its exchange with configuration K is appreciable only above 130 K. Exchange between configurations J and K starts at 110 K.

All the parameters measured from the temperature dependence of the spectra (population of the sites, correlation times k_{ij}^{-1}, rotation barriers) indicate that, in contrast to **R1**, the three potential wells of **R2** are not identical. The variations of the rate constants with $1/T$ show, however, that, in the approximation of the Arrhenius law, the activation energies remain very close to each another and are comprised between 2 and 3 kcal mol^{-1}. A sketch of the principal properties of the potential profile is shown in Figure 7.

The DFT calculated curves visualize some important effects of the hydrocarbon framework on the rotation of the P−H bond around the C(9)−P bond. As expected, passing from the barrelenyl to the triptycyl increases the barrier (interaction with the three benzene protons in β position to C(9)) and using the crystallographic coordinates for **R2′** leave the two potential wells corresponding to configuration J and K very similar whereas the barrier between J and L is drastically dependent upon the orientation of the phenyl ring C(19)−C(24). The comparison between the curves a and d of Figure 5 and that of Figure 7 suggests that after the homolytic scission of the P−H bond a slight reorientation of the phenyl ring increases the barrier between configuration L and J.

Acknowledgment. We thank the Swiss National Science Foundation for financial support.

Supporting Information Available: Tables of atomic coordinates, isotropic and anisotropic displacement parameters, and bond lengths and angles together with *k* and *P* values used for the EPR spectra simulations; EPR spectra obtained at 300 K with a crystal of **2** and **D-2** and at 77 K with a crystal of **D-2**; angular variation of the EPR signals (300 K, crystal of **2**); experimental $1/T$-dependence of the exchange constants for **R2** (11 pages). Ordering and access information is given on any current masthead page.

References and Notes

(1) (a) Oki, M. *Acc. Chem. Res.* **1990**, *23*, 351, (b) Oki, M.; Matsusue, M.; Akinaga, T.; Matsumoto, Y.; Toyota, S. *Bull. Chem. Soc. Jpn.* **1994**, *67*, 2831.

(2) Ramakrishna, G.; Jouaiti, A.; Geoffroy, M.; Bernardinelli, G. *J. Phys. Chem.* **1996**, *100*, 1086.

(3) Nakadaira, Y.; Sato, R.; Sakurai, H. *Chem. Lett.* **1985**, 643.

(4) Kabalka, G. W.; Pagni, R. M. *J. Org. Chem.* **1981**, *46*, 1513.

(5) Blanc, E.; Schwartzenbach, D.; Flack, H. D. *J. Appl. Crystallogr.* **1991**, *24*, 1035.

(6) Main, P.; Fiske, S. J.; Hull, S. E.; Lessinger, L.; Germain, G.; Declercq, J.-P.; Woolfson, M. M. *A System of Computer Programs for the Automatic Solution of Crystal Structures from X-Ray Diffraction Data*; Universities of York, England, and Louvain-la-Neuve, Belgium, 1987.

(7) Hall, S.R.; Flack, H. D.; Stewart, J. M. *Eds XTAL3.2 User's Manual*; Universities of Western Australia and Maryland, 1992.

(8) Johnson, C. K. *ORTEP II*; Report ORNL-5138; Oak Ridge National Laboratory: Oak Ridge, TN, 1976.

(9) Bernardinelli, G; Flack, H. D. *Acta Crystallogr.* **1985**, *A41*, 500.

(10) (a) Hayes, R. G.; Steible, D.; Tolles, W. M.; Hunt, J. *J. Chem. Phys.* **1970**, *53*, 4466. (b) Benetis, N. P.; Sjöquist, L.; Lund, A.; Maruani, J. *J. Magn. Reson.* **1991**, *95*, 523, (c) Heinzer, J. *Mol. Phys.* **1971**, *22*, 167. (d) Bogan, C. M.; Kispert, L. D. *J. Chem. Phys.* **1972**, *57*, 3109.

(11) Frisch, M. J.; Trucks, G. W.; Schlegel, H. B.; Gill, P. M. V.; Johnson, B. G.; Robb, M. A.; Cheeseman, J. R.; Keith, T.; Petersson, G. A.; Montgomery, J. A.; Raghavachari, K.; Al-Laham, M. A.; Zakrzewski, V. G.; Ortiz, J. V.; Foresman, J. B.; Ciolowski, J.; Stefanov, B. B.; Nanayakkara, A.; Challacombe, M.; Peng, C. Y.; Ayala, P. Y.; Chen, W.; Wong, M. W.; Andres, J. L.; Reploges, E. S.; Gomperts R.; Martin R. L.; Fox D. J.; Binkley, J. S.; Defrees D. J.; Baker, J.; Stewart, J. P.; Head-Gordon, M.; Gonzalez, C.; Pople, J. *Gaussian 94*, Revision B.1; Gaussian Inc.: Pittsburgh, PA; 1995.

(12) Wesemann, J.; Jones, P. J.; Schomburg, D.; Heuer, L.; Schmutzler, R. *Chem. Ber.* **1992**, *125*, 2187.

(13) The ^{31}P hyperfine couplings obtained at 300 K are equal to 23, 409, 413 MHz and those measured at 77 K are equal to 4, 74, 848 MHz. Owing to improvement in the precision of our measurements (better estimation of the temperature gradient, more accurate determination of the tensor elements), all the experimental points of the curve $\ln \tau^{-1} = f(1/T)$ are located on a single line and correspond to an energy barrier equal to 2.75 kcal·mol^{-1} (previous results: 3.2 and 1.6 kcal·mol^{-1}).

(14) Bhat, S. N.;. Berclaz, T.; Jouaiti, A.; Geoffroy, M. *Helv. Chim. Acta* **1994**, *77*, 371.